Observation of an α-synuclein liquid droplet state and its maturation into Lewy body-like assemblies

Maarten C. Hardenberg[1], Tessa Sinnige[1], Sam Casford[1], Samuel Dada[1], Chetan Poudel[2], Elizabeth A. Robinson[1], Monika Fuxreiter[3], Clemens Kaminksi[2], Gabriele S. Kaminski Schierle[2], Ellen A. A. Nollen[4], Christopher M. Dobson[1] and Michele Vendruscolo[1]

[1]Centre for Misfolding Diseases, Department of Chemistry,
University of Cambridge, Cambridge CB2 1EW, UK
[2]Department of Chemical Engineering and Biotechnology,
University of Cambridge, Cambridge CB3 0AS, UK
[3]MTA-DE Laboratory of Protein Dynamics,
Department of Biochemistry and Molecular Biology, University of Debrecen, Hungary
[4]University of Groningen, University Medical Centre Groningen,
European Research Institute for the Biology of Aging, Groningen 9713 AV, The Netherlands

Abstract

Misfolded α-synuclein is a major component of Lewy bodies, which are a hallmark of Parkinson's disease. A large body of evidence shows that α-synuclein can aggregate into amyloid fibrils, but the relationship between α-synuclein self-assembly and Lewy body formation remains unclear. Here we show, both *in vitro* and in a *C. elegans* model of Parkinson's disease, that α-synuclein undergoes liquid-liquid phase separation by forming a liquid droplet state, which converts into an amyloid-rich hydrogel with Lewy-body-like properties. This maturation process towards the amyloid state is delayed in the presence of model synaptic vesicles *in vitro*. Taken together, these results suggest that the formation of Lewy bodies may be linked to the arrested maturation of α-synuclein condensates in the presence of lipids and other cellular components.

Introduction

Parkinson's disease (PD) is the most common neurodegenerative movement disorder, affecting over 2% of the world population over 65 years of age (Dawson and Dawson 2003, Poewe, Seppi et al. 2017). The molecular origins of this disease are not fully understood, although they have been closely associated with the aberrant aggregation of α-synuclein (Polymeropoulos, Lavedan et al. 1997, Dawson and Dawson 2003, Singleton, Farrer et al. 2003), a disordered protein whose function appears to involve the regulation of synaptic vesicle trafficking (Burré, Sharma et al. 2010, Bendor, Logan et al. 2013, Fusco, Pape et al. 2016, Lautenschläger, Stephens et al. 2018). This gap in our knowledge of the disease aetiology makes it difficult to choose a target for drug discovery and it is therefore partly responsible for the current lack of disease-modifying therapies for PD (Schapira, Olanow et al. 2014, Dehay, Bourdenx et al. 2015, Valera and Masliah 2016, Brundin, Dave et al. 2017).

The pathological hallmark of PD is the presence of Lewy bodies within dopaminergic neurons in the brains of affected patients (Goedert, Jakes et al. 2017). Although misfolded α-synuclein is a principal constituent of Lewy bodies (Spillantini, Schmidt et al. 1997, Spillantini, Crowther et al. 1998), ultrastructural and proteomic studies have indicated that these aberrant deposits contain a plethora of other cellular components, including lipid membranes and organelle fragments (Arima, Uéda et al. 1998, Spillantini, Crowther et al. 1998, Wakabayashi, Tanji et al. 2013, Shahmoradian, Lewis et al. 2019, Mahul-Mellier, Burtscher et al. 2020). These findings have led to the suggestion that the processes associated with the formation of Lewy bodies could be major drivers of neurotoxicity in PD (Wakabayashi, Tanji et al. 2013, Davis 2020, Mahul-Mellier, Burtscher et al. 2020).

Since it has also been shown that α-synuclein can aggregate into ordered amyloid fibrils *in vitro* (Knowles, Waudby et al. 2009, Cohen, Vendruscolo et al. 2011, Cremades, Cohen et al. 2012, Iljina, Garcia et al. 2016, Li, Ge et al. 2018) and *in vivo* (Ko, Ko et al. 2008, Van Ham, Thijssen et al. 2008, Taschenberger, Garrido et al. 2012, Volpicelli-Daley, Luk et al. 2014, Visanji, Brotchie et al. 2016, Schweighauser, Shi et al. 2020), we asked how such α-synuclein aggregation can be reconciled with the formation of highly complex and heterogeneous assemblies such as Lewy bodies. We hypothesised that α-synuclein may be capable of irreversibly capturing cellular components through liquid-liquid phase separation, as this

63 mechanism has been shown to drive the self-assembly of various disease-associated proteins
64 on-pathway to the formation of solid aggregates (Hyman, Weber et al. 2014, Banani, Lee et al.
65 2017, Shin and Brangwynne 2017, Boeynaems, Alberti et al. 2018). Under healthy conditions,
66 the condensation of proteins into a dense liquid droplet state through liquid-liquid phase
67 separation is normally reversible and exploited in a variety of ways to carry out cellular
68 functions, including RNA metabolism, ribosome biogenesis, DNA damage response and signal
69 transduction (Ader, Frey et al. 2010, Hyman, Weber et al. 2014, Banani, Lee et al. 2017). Upon
70 dysregulation, however, liquid droplets can mature into gel-like deposits, which irreversibly
71 sequester essential cellular components and lead to pathological processes (Patel, Lee et al.
72 2015). This phenomenon has been observed for FUS and TDP-43 in ALS (Murakami, Qamar
73 et al. 2015, Patel, Lee et al. 2015) and for tau in Alzheimer's disease (Ambadipudi, Biernat et
74 al. 2017, Wegmann, Eftekharzadeh et al. 2018, Kanaan, Hamel et al. 2020). Our results show
75 that α-synuclein can undergo a similar process by forming a dense liquid droplet state, which
76 matures into a gel-like state rich in amyloid structure, consistent with recent results (Ray, Singh
77 et al. 2020).
78
79

Results

α-synuclein forms non-amyloid inclusions in *C. elegans*

To understand the initial events in the α-synuclein aggregation process, we assessed its self-association using confocal fluorescence lifetime imaging (FLIM) in the nematode worm *Caenorhabditis elegans*. The fluorescence lifetime of a fluorophore has been previously shown to be an accurate measure of protein self-assembly and amyloid formation, both *in vitro* and in *C. elegans*, and allows amyloid formation to be tracked independent of protein concentration or fluorescence intensity (Kaminski Schierle, Bertoncini et al. 2011, Laine, Sinnige et al. 2019, Poudel, Mela et al. 2020). Given the optical transparency and well-established genetics of *C. elegans*, we sought to compare the fluorescence lifetime of a human α-synuclein-YFP fusion protein stably expressed in body wall muscle cells (OW40 worm model, see **Methods**). As worms do not express native α-synuclein, this model enabled us to specifically study the self-association of human α-synuclein in a cellular context and at known concentrations (±200-300 μM, **Figure S1 and Methods**). In line with previous reports (Van Ham, Thijssen et al. 2008), we observed age-dependent coalescence of α-synuclein-YFP into distinct cytoplasmic inclusions at body wall muscle cells (**Figure 1A** and **Figure S2**). Next, we performed high-resolution FLIM to be able to differentiate the fluorescence lifetime of proteins localised at inclusions from the diffuse (non-aggregated) pool (**Figure 1A**). Our analysis revealed that the self-association state of α-synuclein-YFP in inclusions was similar to that of the diffuse state for the majority of the nematode's adult life (days 1-11 of adulthood), indicating that the early α-synuclein assemblies are predominantly non-amyloid in *C. elegans* (**Figure 1B, C**). Only at old age, α-synuclein-YFP inclusions started to show increased amyloid-like features (days 13-15 of adulthood), an observation supported by the simultaneous appearance of proteinase K resistant protein species (**Figure 1D**). In addition to the presence of amyloid features, we found that the majority of inclusions at old age (day 15) were immunoreactive for ubiquitin, which is characteristic of α-synuclein deposits in PD (**Figure 2A-C**). By contrast, ubiquitin is not found in inclusions of younger animals (day 7). This is expected as post-translational modifications, such as ubiquitination, occur later on in PD pathogenesis, and indicates the presence of aggregated α-synuclein species (Mahul-Mellier, Burtscher et al. 2020). Together, our FLIM analysis shows that α-synuclein predominantly resides in mobile, non-amyloid inclusions, which is in agreement with previous studies (Van Ham, Thijssen et al. 2008, Kaminski

112   Schierle, Bertoncini et al. 2011, Laine, Sinnige et al. 2019, Poudel, Mela et al. 2020), before

113   transitioning into amyloid and ubiquitin positive deposits.

114

Early α-synuclein inclusions in *C. elegans* have liquid-like properties

116   The presence of non-amyloid α-synuclein assemblies in *C. elegans* prompted us to further

117   investigate their material properties. To this end, we used the aliphatic alcohol 1,6-hexanediol,

118   which has recently been used as a tool to test the liquid properties of protein condensates *in*

119   *vitro* as well as *in vivo* (Kroschwald, Maharana et al. 2017). Hexanediol dissolves assemblies

120   maintained by weak hydrophobic interactions, whereas solid-like amyloid structures remain

121   intact. Exposure to 10% (w/v) hexanediol in *C. elegans* almost completely dissolved α-

122   synuclein inclusions between days 1 and 11 of adulthood, reflecting the role of low-affinity

123   interactions in inclusion assembly (**Figure 3A, B** and **Movie S1**). As before, inclusions in aged

124   nematodes (days 13-15 of adulthood) appeared to be amyloid-like, as evidenced by decreased

125   hexanediol-mediated dissipation. We then assessed whether α-synuclein assemblies in younger

126   nematodes could reappear after hexanediol was washed out. Indeed, newly formed small

127   inclusions were observed in washed worms after one day of recovery, reflecting the dynamic

128   and liquid-like properties of α-synuclein assemblies in *C. elegans* (**Figure 3C, D**). To validate

129   our observations, we tested the liquid properties of α-synuclein assemblies using FRAP

130   (**Figure 3E-G**). We found that α-synuclein at inclusions was liquid up until day 11 of

131   adulthood, as evidenced by rapid recovery after photobleaching. Further ageing, however,

132   resulted in a decline in FRAP which confirms the observed transition from liquid to solid-like

133   α-synuclein inclusions.

134

Liquid-liquid phase separation drives α-synuclein droplet formation *in vitro*

136   The results presented above indicate that α-synuclein is a component of liquid-like assemblies

137   in *C. elegans*. To investigate whether this behaviour is mediated by the intrinsic biophysical

138   properties of α-synuclein, we tested its capability of forming such assemblies *in vitro*. We

139   incubated Alexa-488 labelled human α-synuclein at physiological pH and in the presence of

140   polyethylene glycol (PEG 12,000), a commonly used crowding agent that does not affect the

141   unfolded conformation of α-synuclein (A. Munishkina, M. Cooper et al. 2004, C. Mcnulty,

142   B. Young et al. 2006) (**Methods**). When deposited on a glass surface, α-synuclein formed

143   micron-sized droplets within several minutes (**Figures 4A** and **Movie S2**), at concentrations

144   that can be found at the pre-synaptic terminal (±50-100 μM) as well as concentrations

145   associated with pathological overexpression (>100 μM) (**Figure S3**) (R. Bodner, M. Dobson

146   et al. 2009, G. Wilhelm, S. Mandad et al. 2014). Droplet formation was sensitive to ionic

147   strength (**Figure S4**), which is likely the result of the involvement of the acidic C-terminal

148   region of α-synuclein. We predicted that this region can spontaneously phase separate via

149   disordered interactions (**Figure S5**), which are likely involved in the stabilisation of the droplet

150   in conjunction with hydrophobic effects mediated by the NAC region (Ray, Singh et al. 2020).

151   To characterise whether α-synuclein droplets had properties of a liquid phase, we assessed two

152   key biophysical features. First, we observed that two droplets readily fuse and relax into a

153   larger droplet once they come in close proximity (<1 μm) (**Figure 4B** and **Movie S3**). Second,

154   fluorescence recovery after photobleaching (FRAP) of a small area within the droplet was

155   followed by rapid recovery ($t_{1/2}$ = 5 s), reflecting local rearrangement of α-synuclein molecules

156   within the condensate (**Figure 4C** and **Movie S4**).

157

158   **The conversion of α-synuclein droplets into gel-like assemblies is associated with amyloid**

159   **formation**

160   The ability of α-synuclein molecules to rearrange within droplets declines over time (**Figure**

161   **4C**), which is in line with the thermodynamic drive of dense protein solutions to mature into

162   more solid-like states, such as highly ordered amyloid fibrils (Molliex, Temirov et al. 2015,

163   Patel, Lee et al. 2015, Harmon, Holehouse et al. 2017, Wegmann, Eftekharzadeh et al. 2018).

164   To test whether the maturation of α-synuclein droplets is associated with amyloid formation,

165   we assessed this process using turbidity measurements in the presence of the amyloid-binding

166   dye thioflavin T (ThT) (**Figure 5A, B**). Droplet formation as seen from increased turbidity at

167   540 nm was followed by increased ThT fluorescence, indicating that droplet ageing involves

168   the formation of amyloid species. Furthermore, a hydrogel with amyloid-like features could be

169   recovered at the end of each incubation period (**Figure 5C**). These results indicate that under

170   physiological conditions, α-synuclein can undergo a phase transition into a dynamic liquid

171   droplet state which converts into gel-like aggregates over time.

172

173   **α-Synuclein droplets age more slowly when merged with liposomes**

174   In dopaminergic neurons, α-synuclein is highly concentrated at pre-synaptic terminals where

175   it can transiently bind a variety of lipid surfaces, including those of synaptic vesicles (Burré,

176   Sharma et al. 2010, Burré, Sharma et al. 2014, Fusco, Pape et al. 2016, Lautenschläger,

177   Stephens et al. 2018). These observations lead to the question of whether synaptic vesicles

178 modulate the phase behaviour of α-synuclein. We thus incubated α-synuclein with liposomes

179 with a composition mimicking that of synaptic vesicles (Takamori, Holt et al. 2006)

180 (**Methods**). To enable detection by fluorescence microscopy, liposomes were supplemented

181 with a fluorescently labelled lipid, 1,2-dioleoyl-sn-glycero-3-phosphoethanolamine-N-

182 (cyanine 5) (Cy5-DOPE) (**Methods**). Formation of α-synuclein droplets coincided with the

183 appearance of condensates that were positive for the labelled lipid (**Figure 6A** and **Movie S5**),

184 whereas liposomes alone either remained diffuse or formed irregular aggregates (**Figure 6B**).

185 Co-localisation of lipids and α-synuclein at droplets was dependent on the protein:lipid ratio

186 (**Figure 6A)**, where a higher ratio resulted in reduced mixing of liposomes and α-synuclein

187 (**Figure 6A, bottom**). 3D rendering of the droplets showed that lipids are directly recruited

188 into α-synuclein droplets (**Figure 6C** and **Movie S6**), in which α-synuclein continues to

189 behave as a liquid phase as evidenced by rapid fusion of two α-synuclein/lipid droplets (**Figure**

190 **6D**). Crucially, α-synuclein/lipid droplets appeared to be more resistant to ageing, as the

191 protein in these mixed droplets showed a slower decline in FRAP when compared to pure α-

192 synuclein droplets (**Figure 6E**). This effect was lost when the concentration of liposomes was

193 reduced. We also note that the lipids inside the droplets have limited FRAP, suggesting that

194 they are either restricted in their mobility or stabilised upon interaction with α-synuclein

195 (**Figure 6E, bottom**). Taken together, these results suggest that liposomes mimicking synaptic

196 vesicles stabilise the liquid state of α-synuclein, which could reflect the native environment of

197 α-synuclein where synaptic membranes are highly abundant. Indeed, reduced aggregation in

198 the presence of synaptic membranes is expected as the binding of α-synuclein to these

199 membranes does not readily trigger amyloid formation *in vitro* (Galvagnion, Brown et al.

200 2016). In this context, the binding of α-synuclein to the surface of liposomes likely reduces the

201 amount of α-synuclein available to engage in β-sheet formation, consistent with the law of

202 mass action. A converse effect can be observed for membranes with primarily charged

203 headgroups, which have an overall aggregation promoting effect, (Galvagnion, Brown et al.

204 2016) and have been shown to accelerate ageing of α-synuclein droplets (Ray, Singh et al.

205 2020).

206

207

Discussion and Conclusions

We have shown that α-synuclein forms liquid-like condensates *in vivo* in a *C. elegans* model of PD and *in vitro* at physiological concentrations and pH. Our FLIM analysis indicated that the inclusions formed by α-synuclein in *C. elegans* body wall muscle cells are largely non-amyloid and can be dissociated by 1,6-hexanediol. α-Synuclein droplets behave as a liquid phase *in vitro*, as individual α-synuclein molecules rapidly rearrange within the droplets, and individual droplets were observed to fuse and relax back into a spherical shape.

These observations can be linked to the increasing evidence that the phenomenon of liquid-liquid phase separation underlies the organisation of proteins at the synapse (Milovanovic, Wu et al. 2018, Chen, Wu et al. 2020, Chen, Wu et al. 2020). It has also been shown that α-synuclein clusters synaptic vesicles and regulates the synaptic vesicle pool (Burré, Sharma et al. 2010, Bendor, Logan et al. 2013, Fusco, Pape et al. 2016, Lautenschläger, Stephens et al. 2018). In this context, our results suggest that droplet formation by α-synuclein may be involved in a physiological mechanism to cluster synaptic vesicles, possibly in conjunction with other proteins such as synapsins, which have also been shown to phase-separate into liquid-like assemblies (Milovanovic, Wu et al. 2018). Indeed, synapsins are implicated in synaptic function in conjunction with synuclein (Zaltieri, Grigoletto et al. 2015, Atias, Tevet et al. 2019) and are components of Lewy bodies (Longhena, Faustini et al. 2018).

We have also shown that the droplet state can undergo a maturation process into a gel-like state rich in amyloid structure and immunoreactive for ubiquitin, which is reminiscent of the pathological state seen in Lewy body pathologies (Spillantini, Schmidt et al. 1997, Spillantini, Crowther et al. 1998, Araki, Yagi et al. 2019). This phenomenon is expected on the grounds that the transition from the droplet state to the amyloid state takes place through a maturation process, known as Ostwald step rule (Boke, Ruer et al. 2016, Yuan, Levin et al. 2019), and it is consistent with the recent report that α-synuclein can form hydrogels (Kumar, Das et al. 2018, Pogostin, Linse et al. 2019). From a thermodynamic point of view, it is important to note that the gel-like assembly is not a stable state in addition to the native, the droplet and the amyloid states, but a slowly evolving conformation on pathway to the amyloid state (**Figure 6A**). This ageing process can become very slow depending on the complexity of the composition, and one can speculate that Lewy bodies are in a condition of nearly arrested

241 maturation. In this context, we found that the sequestration of liposomes mimicking synaptic
242 vesicles slows the maturation process, which is consistent with the observation that various
243 lipid vesicles and membranes are found in Lewy bodies (Shahmoradian, Lewis et al. 2019,
244 Mahul-Mellier, Burtscher et al. 2020). We can thus suggest that the effects of such
245 membranous structures on the ageing process of the droplets involve a slowing down of the
246 amyloid conversion of the gel-like α-synuclein assemblies. This process could create a
247 metastable toxic state, as gel-like assemblies are a reservoir for cytotoxic α-synuclein
248 oligomers (Kumar, Das et al. 2018).

249

250 We also note that the conversion of α-synuclein between the native state and the amyloid state
251 can take place directly through a 'deposition pathway' (**Figure 7B**) following a more
252 conventional nucleation-growth process (Buell, Galvagnion et al. 2014), where the nucleation
253 step can be catalysed by the presence of charged lipid membranes (Galvagnion, Buell et al.
254 2015), rather than the 'condensation pathway' described here (**Figure 7B**). Whether α-
255 synuclein primarily follows the deposition route to the amyloid state or the condensation route
256 through the droplet state is likely determined by the environmental conditions. One such
257 condition could involve the lipid composition of membranes, since this determines the rate of
258 α-synuclein nucleation, with membranes mimicking synaptic vesicles being unable to drive
259 nucleation (Galvagnion, Brown et al. 2016). A decline in synaptic vesicles density, as observed
260 for some PD mutations through altered synaptic protein function (Nguyen and Krainc 2018),
261 could therefore shift α-synuclein membrane binding with adverse consequences.

262

263 In conclusion, we have shown that α-synuclein undergoes liquid-liquid phase separation to
264 adopt a droplet state and that this process may lead to the formation of aberrant gel-like
265 assemblies with features of Lewy bodies.

266
267

Materials and Methods

C. elegans strains and maintenance

Standard conditions were used for the propagation of *C. elegans* (Goldstein 2016). We used the OW40 (zgIs15[unc-54p::α-synuclein::YFP] IV) strain in which α-synuclein is fused to yellow fluorescent protein (YFP) and stably expressed in body wall muscle cells (Van Ham, Thijssen et al. 2008). OW40 animals were synchronised by hypochlorite bleaching, hatched overnight in M9 buffer (3 g/L KH_2PO_4, 6 g/L Na_2HPO_4, 5 g/L NaCl, 1 mM $MgSO_4$) and subsequently cultured at 20 °C on nematode growth medium (NGM) plates (1 mM $CaCl_2$, 1 mM $MgSO_4$, 5 μg/mL cholesterol, 250 mM KH_2PO_4 [pH 6], 17 g/L agar, 3 g/L NaCl, 7.5 g/L casein), which were seeded with the *Escherichia coli* strain OP50. At L4 stage, larvae were placed on nematode growth medium (NGM) plates containing 5-fluoro- 2'deoxy-uridine (FUDR, Sigma) (75 μM) to inhibit the growth of offspring.

Estimation of *C. elegans* α-synuclein concentration

To estimate the concentration of α-synuclein at the *C. elegans* body wall muscle cells, 50 worms were hand-picked into 1X Laemmli buffer and heated at 100 °C for 5 minutes. Simultaneously, known concentrations of purified human α-synuclein (see **α-synuclein purification and labelling**) were diluted in 1X Laemmli buffer and heated at 100 °C for 5 minutes. Resulting protein solutions were then separated on a NuPAGE Novex 4-12 % Bis-Tris Protein Gels (Life Technologies) and transferred to nitrocellulose membranes using an iBlot Dry Blotting System (Life Technologies). To improve α-synuclein immunodetection, the membrane was treated with phosphate-buffered saline (PBS) containing 0.4% paraformaldehyde for 30 min at room temperature, followed by blocking for 1 h with 5% skim milk in PBS. Membranes were probed with the LB509 anti-α-synuclein antibody (1:1000; Abcam) overnight at 4 °C and visualised with a fluorescent secondary antibody (goat-anti-mouse IgG Alexa 488-conjugated (1:5000, A11029, Life Technologies)). Fluorescent bands were detected on a Typhoon FLA 7000 (GE Life Sciences) imaging system and quantified in ImageJ (NIH). To determine the protein content per cell, α-synuclein levels were compared to the purified α-synuclein standard and the resulting value was divided by the number of cells in which the protein is expressed under the unc-54 promoter (95 body wall muscle cells, 8 vulval muscle cells and anal depressor cell). Finally, the volume of each cell used to calculate the final concentration was ±1pL, as previously determined (Sinnige, Meisl et al. 2020).

Fluorescence lifetime imaging (FLIM)

At indicated timepoints, transgenic worms were washed off NGM plates in M9 buffer and mounted on 2.5% agarose pads on glass microscopy slides and immobilised using 10 mM levamisole hydrochloride (Merck). Slides were then mounted onto a modified, confocal-based platform (Olympus FV300-IX700) integrated with a time-correlated single photon counting (TCSPC) module (SPC-830, B&H). Images of the anterior region of the worm were acquired at 60X (PLAPON 60XOSC2, 1.4NA, Olympus) magnification. For excitation of YFP, the output of a pulsed supercontinuum source (WL-SC-400-15, Fianium Ltd.) operating at 40 MHz repetition rate and filtered using a FF03-510/20 (Semrock Inc.) bandpass filter was used. YFP fluorescence emission was filtered with a FF01-542/27 (Semrock Inc.) bandpass filter. Photons were acquired for two minutes to create a single 256×256 image with 256 time bins. Inclusions were detected using a custom-designed image-processing pipeline in ImageJ (NIH). Briefly, cytoplasmic background was reduced through application of a Gaussian convolution filter and binarised according to the Chow and Kaneko adaptive thresholding method (Chow and Kaneko 1972). Subsequently, clustered inclusions were separated using a classic watershed segmentation algorithm. The resulting image was then used to create a mask of the signal representing inclusions and subtracted from the total signal, creating a separate mask for the diffuse signal. Lifetime analysis of the processed images was carried out using FLIMFit (Imperial College London Photonics). FLIM data were fitted with a single exponential decay function to extract the fluorescence lifetime in each pixel using FLIMFit v4.12 (Warren, Margineanu et al. 2013).

Proteinase K assay

For proteinase K digestion assays, worms were lysed using a Balch homogeniser in NP-40 lysis buffer (150 mM NaCl, 1.0% NP-40, 50 mM Tris pH 8.0), as described previously (Bhaskaran, Butler et al. 2011). Lysates were kept on ice before being exposed to increasing proteinase K concentrations (0, 1, 2, 3 µg/µl) for 30 minutes at 37 °C. Following digestion, samples were immediately heated at 100 °C for 5 minutes in Laemmli buffer, separated on NuPAGE Novex 4-12 % Bis-Tris Protein Gels (Life Technologies) and transferred to nitrocellulose membranes using an iBlot Dry Blotting System (Life Technologies). To improve α-synuclein immunodetection, the membrane was treated with phosphate-buffered saline (PBS) containing 0.4% paraformaldehyde for 30 min at room temperature, followed by blocking for 1 h with 5% skim milk in PBS. Membranes were probed with the LB509 anti-α-synuclein antibody (1:1000;

335   Abcam) overnight at 4 °C and visualised with a fluorescent secondary antibody (goat-anti-
336   mouse IgG Alexa 488-conjugated (1:5000, A11029, Life Technologies)). Fluorescent bands
337   were detected on a Typhoon FLA 7000 (GE Life Sciences) imaging system. Images were
338   quantified in ImageJ (NIH).
339

340   **Ubiquitin antibody staining**
341   For ubiquitin antibody staining in *C. elegans*, animals were washed off NGM plates in M9
342   buffer and transferred to Eppendorf tubes. Worms were fixed in three consecutive steps to
343   prevent disturbing the liquid-like inclusions, while also maintaining structure and epitope
344   availability; First worms were briefly exposed to ice-cold methanol (5 min, on ice), followed
345   by ice-cold acetone (5 min, on ice), before incubation with 4% paraformaldehyde (Thermo
346   Fisher, Pierce) (20 min, at room temperature). Worms were washed with PBS in between each
347   fixation step, avoiding the use of centrifugation by letting the worms sediment on the bottom
348   of the tube. Following fixation, animals were incubated with 1 ml of Alexa Fluor 647-
349   conjugated anti-ubiquitin antibody (1:200, Abcam) for 1 hour at room temperature. Excess
350   antibody was removed by 3 PBS washes as described above, after which animals were
351   embedded in 50 μL of a thermo-reversible hydrogel (CyGEL^{TM}, Biostatus) and imaged on a
352   Leica TCS SP8 inverted confocal microscope using a 40x/1.3 HC PL Apo CS oil objective
353   (Leica Microsystems). Sequential line scanning was used to avoid bleed through of the YFP
354   signal.
355

356   **Hexanediol experiments**
357   To achieve slow diffusion of 1,6-hexanediol into the worms without eliciting rapid toxic
358   effects, animals were washed off NGM plates in M9 buffer and embedded in 20 μL of a thermo-
359   reversible hydrogel (CyGEL^{TM}, Biostatus) supplemented with 10% (w/v) 1,6-hexanediol
360   (Sigma) and 10 mM levamisole hydrochloride (Merck) on a glass-bottom imaging dish
361   (MatTek P35G-1.5-14-C). For control experiments, worms were embedded in hydrogel with
362   10% dH$_2$O and 10 mM levamisole hydrochloride. Glass-bottom dishes were subsequently
363   sealed with a 12 mm x 12 mm 1.5 cover glass (Fisherbrand) and left at room temperature for 1
364   hour. After incubation, worms were imaged on a Leica SP8 upright confocal microscope using
365   a 40x/1.3 HC PL Apo CS oil objective (Leica Microsystems). For recovery experiments,
366   imaging dishes were cooled on ice until the hydrogel liquified and immediately diluted in M9

buffer. Worms were then washed 2x in M9 buffer, before being left to recover on seeded NGM
plates for 24 hours. Hereafter, worms were imaged as described above.

α-synuclein purification and labelling

Wild type and A90C α-synuclein were purified from *E. coli* expressing plasmid pT7-7
encoding for the protein as previously described (Hoyer, Antony et al. 2002, Cremades, Cohen
et al. 2012). Following purification, the protein was concentrated using Amicon Ultra-15
Centrifugal Filter Units (Merck Millipore). A90C α-synuclein was labelled with 1.5-fold molar
excess Alexa Fluor 488 C_5 maleimide (Life Technologies) overnight at 4 °C. The excess dye
was removed on a Sephadex G-25 desalting column (Sigma) as described previously
(Cremades, Cohen et al. 2012), and buffer exchanged into 25 mM Tris-HCl (pH 7.4).

Liquid-liquid phase separation assay

To induce droplet formation, non-labelled wild type α-synuclein was mixed with Alexa Fluor
488 labelled A90C α-synuclein at a 10:1 molar ratio in 25 mM Tris-HCl (pH 7.4), 50 mM
NaCl, 1 mM DTT and 10% polyethylene glycol 12,000 (PEG) (Thermo Fisher Scientific) at
20 °C, unless indicated otherwise. The final mixture was pipetted on a 35 mm glass-bottom
dish (P35G-1.5-20-C, MatTek Life Sciences) and immediately imaged on a Leica TCS SP5
confocal microscope using a 40x/1.3 HC PL Apo CS oil objective (Leica Microsystems). The
excitation wavelength was 488 nM for all experiments. All images were processed and
analysed in ImageJ (NIH).

Fluorescence recovery after photobleaching

Fluorescence recovery after photobleaching (FRAP) was performed on the setup described
above for the liquid-liquid phase separation assay, under the same experimental conditions.
Bleaching was done using the 488 nm laser at 50% intensity, to obtain ±50-60% relative
photobleaching. Images were captured at 600 ms intervals, following a 1.8 s (3 frame) pre-
bleach sequence and a 1.2 s (2 frame) spot bleach covering 30-50% of the droplet area.
Intensity traces of the bleached area were background corrected and normalised.

For *C. elegans* experiments, worms were immobilised in 20 µL CyGEL™ (Biostatus)
supplemented with 10 mM levamisole hydrochloride (Merck) and placed on a glass-bottom
imaging dish (MatTek P35G-1.5-14-C).

Liposome preparation

Small unilamellar vesicles (SUVs) were prepared to approximate the lipid composition of synaptic vesicles (Takamori, Holt et al. 2006), 50 mol% DOPC (1,2-dioleoyl-sn-glycero-3-phosphocholine), 30 mol% DOPE (1,2-dioleoyl-sn-glycero-3-phosphatidylethanolamine), 20 mol% DOPS (1,2-dioleoyl-sn-glycero-3-phospho-L-serine), and supplemented with 1 mol% DOPE-Cy5 (1,2-dioleoyl-sn-glycero-3-phosphoethanolamine-N-(Cyanine 5)) (Avanti Polar Lipids). Lipids were mixed in chloroform and dried under a mild stream of nitrogen gas. Dried lipids were then lyophilised for 3 h (VWR, Avantor), before being rehydrated in 25 mM Tris-HCl (pH 7.4). Liposomes were formed by ten consecutive freeze-thaw cycles (-196 °C to 30°C). To form uniformly sized liposomes, the mixture was extruded 20 times through 50 nm-diameter polycarbonate filters (Avanti Polar Lipids). Liposome size distribution was confirmed using dynamic light scattering (Average size ± 50 nm) and re-extruded when standard deviation > 20 nm.

Turbidity and thioflavin T (ThT) assay

Wild type α-synuclein was mixed with 20 μM ThT in 25 mM Tris-HCl (pH 7.4), 50 mM NaCl, and 10% PEG 12,000 (Thermo Fisher Scientific) at 20 °C. All samples were prepared in low binding test tubes (Eppendorf), after which each sample was pipetted in triplicate into a 96-well half-area, low-binding, clear bottom plate (Corning) on ice?. Assays were initiated by placing the 96-well plate at 20 °C under intermediate (5 min) shaking (100 rpm, 10 s) conditions in a plate reader (Fluostar Omega or Fluostar Optima, BMG Labtech). The absorbance at 540 nm was measured every 5 min over 72 h. ThT fluorescence was measured through the bottom of the plate with a 440 nm excitation filter and a 480 nm emission filter.

Electron microscopy (cryo-SEM)

Cryo-SEM was performed on a Verios 460 scanning electron microscope (FEI/Thermo Fisher) equipped with a Quorum PP3010T cryo-transfer system. Hydrogel samples were pipetted into shuttle-mounted universal cryo-stubs and flash-frozen in slushed nitrogen. After transfer into the prep-chamber, samples were fractured, sublimed at -90 °C for 2 minutes, sputter-coated with a thin layer of platinum and transferred to the SEM cryo-stage. Both prep-chamber and cryo-stage were set to -140 °C. SE-imaging was performed at 1 keV accelerating voltage and 25 pA probe current using the Through-Lens-Detector (TLD) in immersion mode. Images

432   were acquired with a pixel resolution of 1536 x 1024 pixels using a 300 ns dwell time/32 image

433   integrations and using drift correction.

434

435   **Droplet predictions**

436   The binding modes of α-synuclein, as the probability to undergo disorder-to-order (p_{DO}) or

437   disorder-to-disorder (p_{DD}) transitions upon interactions, were predicted from the amino acid

438   sequence using the FuzPred program (protdyn-fuzpred.org) (Miskei, Horváth et al. 2020). The

439   FuzPred-Droplet method was used to estimate the probability for spontaneous liquid-liquid

440   phase separation based on disorder in the free and bound states.

441

442   **Statistical analysis**

443   All statistical analysis was performed in GraphPad Prism 8 (GraphPad Software). Data are

444   presented as means ± SEM from at least 3 independent biological replicates, unless indicated

445   otherwise. Statistical significance between experimental groups was analysed either by 2-tailed

446   Student's *t* test or one-way ANOVA followed by Bonferroni's multiple-comparison

447

457
458

References

A. Munishkina, L., E. M. Cooper, V. N. Uversky and A. L. Fink (2004). "The effect of macromolecular crowding on protein aggregation and amyloid fibril formation." Journal of Molecular Recognition **17**(5): 456-464.

Ader, C., S. Frey, W. Maas, H. B. Schmidt, D. Görlich and M. Baldus (2010). "Amyloid-like interactions within nucleoporin FG hydrogels." Proceedings of the National Academy of Sciences **107**(14): 6281-6285.

Ambadipudi, S., J. Biernat, D. Riedel, E. Mandelkow and M. Zweckstetter (2017). "Liquid–liquid phase separation of the microtubule-binding repeats of the Alzheimer-related protein Tau." Nature communications **8**(1): 1-13.

Araki, K., N. Yagi, K. Aoyama, C.-J. Choong, H. Hayakawa, H. Fujimura, Y. Nagai, Y. Goto and H. Mochizuki (2019). "Parkinson's disease is a type of amyloidosis featuring accumulation of amyloid fibrils of α-synuclein." Proceedings of the National Academy of Sciences **116**(36): 17963-17969.

Arima, K., K. Uéda, N. Sunohara, S. Hirai, Y. Izumiyama, H. Tonozuka-Uehara and M. Kawai (1998). "Immunoelectron-microscopic demonstration of NACP/α-synuclein-epitopes on the filamentous component of Lewy bodies in Parkinson's disease and in dementia with Lewy bodies." Brain Research **808**(1): 93-100.

Atias, M., Y. Tevet, J. Sun, A. Stavsky, S. Tal, J. Kahn, S. Roy and D. Gitler (2019). "Synapsins regulate α-synuclein functions." Proceedings of the National Academy of Sciences **116**(23): 11116-11118.

Banani, S. F., H. O. Lee, A. A. Hyman and M. K. Rosen (2017). "Biomolecular condensates: organizers of cellular biochemistry." Nature reviews Molecular cell biology **18**(5): 285-298.

Bendor, J. T., T. P. Logan and R. H. Edwards (2013). "The function of α-synuclein." Neuron **79**(6): 1044-1066.

Bhaskaran, S., J. A. Butler, S. Becerra, V. Fassio, M. Girotti and S. L. Rea (2011). "Breaking Caenorhabditis elegans the easy way using the Balch homogenizer: an old tool for a new application." Analytical biochemistry **413**(2): 123-132.

Boeynaems, S., S. Alberti, N. L. Fawzi, T. Mittag, M. Polymenidou, F. Rousseau, J. Schymkowitz, J. Shorter, B. Wolozin and L. Van Den Bosch (2018). "Protein phase separation: a new phase in cell biology." Trends in cell biology **28**(6): 420-435.

491 Boke, E., M. Ruer, M. Wühr, M. Coughlin, R. Lemaitre, S. P. Gygi, S. Alberti, D. Drechsel,
492 A. A. Hyman and T. J. Mitchison (2016). "Amyloid-like self-assembly of a cellular
493 compartment." Cell **166**(3): 637-650.

494 Brundin, P., K. D. Dave and J. H. Kordower (2017). "Therapeutic approaches to target alpha-
495 synuclein pathology." Experimental neurology **298**: 225-235.

496 Buell, A. K., C. Galvagnion, R. Gaspar, E. Sparr, M. Vendruscolo, T. P. Knowles, S. Linse and
497 C. M. Dobson (2014). "Solution conditions determine the relative importance of nucleation
498 and growth processes in α-synuclein aggregation." Proceedings of the National Academy of
499 Sciences **111**(21): 7671-7676.

500 Burré, J., M. Sharma and T. C. Südhof (2014). "α-Synuclein assembles into higher-order
501 multimers upon membrane binding to promote SNARE complex formation." Proceedings of
502 the National Academy of Sciences **111**(40): E4274-E4283.

503 Burré, J., M. Sharma, T. Tsetsenis, V. Buchman, M. R. Etherton and T. C. Südhof (2010). "α-
504 Synuclein promotes SNARE-complex assembly in vivo and in vitro." Science **329**(5999):
505 1663-1667.

506 C. Mcnulty, B., G. B. Young and G. J. Pielak (2006). "Macromolecular Crowding in the
507 Escherichia coli Periplasm Maintains α-Synuclein Disorder." Journal of Molecular Biology
508 **355**(5): 893-897.

509 Chen, X., X. Wu, H. Wu and M. Zhang (2020). "Phase separation at the synapse." Nature
510 Neuroscience: 1-10.

511 Chen, X., X. Wu, H. Wu and M. Zhang (2020). "Phase separation at the synapse." Nature
512 Neuroscience.

513 Chow, C. and T. Kaneko (1972). "Automatic boundary detection of the left ventricle from
514 cineangiograms." Computers and biomedical research **5**(4): 388-410.

515 Cohen, S. I. A., M. Vendruscolo, C. M. Dobson and T. P. J. Knowles (2011). "Nucleated
516 polymerization with secondary pathways. II. Determination of self-consistent solutions to
517 growth processes described by non-linear master equations." The Journal of Chemical Physics
518 **135**(6): 065106.

519 Cremades, N., S. I. Cohen, E. Deas, A. Y. Abramov, A. Y. Chen, A. Orte, M. Sandal, R. W.
520 Clarke, P. Dunne and F. A. Aprile (2012). "Direct observation of the interconversion of normal
521 and toxic forms of α-synuclein." Cell **149**(5): 1048-1059.

522 Davis, A. A. (2020). "Beyond synuclein: Organelle accumulation in Lewy bodies may drive
523 neurodegeneration." Science Translational Medicine **12**(536): eabb2778.

524 Dawson, T. M. and V. L. Dawson (2003). "Molecular pathways of neurodegeneration in
525 Parkinson's disease." Science **302**(5646): 819-822.

526 Dehay, B., M. Bourdenx, P. Gorry, S. Przedborski, M. Vila, S. Hunot, A. Singleton, C. W.
527 Olanow, K. M. Merchant and E. Bezard (2015). "Targeting α-synuclein for treatment of
528 Parkinson's disease: mechanistic and therapeutic considerations." The Lancet Neurology **14**(8):
529 855-866.

530 Fusco, G., T. Pape, A. D. Stephens, P. Mahou, A. R. Costa, C. F. Kaminski, G. S. K. Schierle,
531 M. Vendruscolo, G. Veglia and C. M. Dobson (2016). "Structural basis of synaptic vesicle
532 assembly promoted by α-synuclein." Nature communications **7**(1): 1-12.

533 G. Wilhelm, B., S. Mandad, S. Truckenbrodt, K. Krohnert, C. Schafer, B. Rammner, S. J. Koo,
534 G. A. Classen, M. Krauss, V. Haucke, H. Urlaub and S. O. Rizzoli (2014). "Composition of
535 isolated synaptic boutons reveals the amounts of vesicle trafficking proteins." Science
536 **344**(6187): 1023-1028.

537 Galvagnion, C., J. W. Brown, M. M. Ouberai, P. Flagmeier, M. Vendruscolo, A. K. Buell, E.
538 Sparr and C. M. Dobson (2016). "Chemical properties of lipids strongly affect the kinetics of
539 the membrane-induced aggregation of α-synuclein." Proceedings of the National Academy of
540 Sciences **113**(26): 7065-7070.

541 Galvagnion, C., A. K. Buell, G. Meisl, T. C. Michaels, M. Vendruscolo, T. P. Knowles and C.
542 M. Dobson (2015). "Lipid vesicles trigger α-synuclein aggregation by stimulating primary
543 nucleation." Nature chemical biology **11**(3): 229.

544 Goedert, M., R. Jakes and M. G. Spillantini (2017). "The synucleinopathies: twenty years on."
545 Journal of Parkinson's disease **7**(s1): S51-S69.

546 Goldstein, B. (2016). "Sydney Brenner on the Genetics of Caenorhabditis elegans." Genetics
547 **204**(1): 1.

548 Harmon, T. S., A. S. Holehouse, M. K. Rosen and R. V. Pappu (2017). "Intrinsically disordered
549 linkers determine the interplay between phase separation and gelation in multivalent proteins."
550 Elife **6**: e30294.

551 Hoyer, W., T. Antony, D. Cherny, G. Heim, T. M. Jovin and V. Subramaniam (2002).
552 "Dependence of α-synuclein aggregate morphology on solution conditions." Journal of
553 molecular biology **322**(2): 383-393.

554 Hyman, A. A., C. A. Weber and F. Jülicher (2014). "Liquid-liquid phase separation in biology."
555 Annual review of cell and developmental biology **30**: 39-58.

556 Iljina, M., G. A. Garcia, M. H. Horrocks, L. Tosatto, M. L. Choi, K. A. Ganzinger, A. Y.
557 Abramov, S. Gandhi, N. W. Wood, N. Cremades, C. M. Dobson, T. P. J. Knowles and D.

Klenerman (2016). "Kinetic model of the aggregation of alpha-synuclein provides insights into prion-like spreading." Proceedings of the National Academy of Sciences **113**(9): E1206-E1215.

Kaminski Schierle, G. S., C. W. Bertoncini, F. T. Chan, A. T. van der Goot, S. Schwedler, J. Skepper, S. Schlachter, T. van Ham, A. Esposito and J. R. Kumita (2011). "A FRET sensor for non-invasive imaging of amyloid formation in vivo." ChemPhysChem **12**(3): 673-680.

Kanaan, N. M., C. Hamel, T. Grabinski and B. Combs (2020). "Liquid-liquid phase separation induces pathogenic tau conformations in vitro." Nature Communications **11**(1).

Knowles, T. P. J., C. A. Waudby, G. L. Devlin, S. I. A. Cohen, A. Aguzzi, M. Vendruscolo, E. M. Terentjev, M. E. Welland and C. M. Dobson (2009). "An Analytical Solution to the Kinetics of Breakable Filament Assembly." Science **326**(5959): 1533-1537.

Ko, L. W., H. H. Ko, W. L. Lin, J. G. Kulathingal and S. H. Yen (2008). "Aggregates assembled from overexpression of wild-type alpha-synuclein are not toxic to human neuronal cells." J Neuropathol Exp Neurol **67**(11): 1084-1096.

Kroschwald, S., S. Maharana and A. Simon (2017). "Hexanediol: a chemical probe to investigate the material properties of membrane-less compartments." Matters **3**(5): e201702000010.

Kumar, R., S. Das, G. M. Mohite, S. K. Rout, S. Halder, N. N. Jha, S. Ray, S. Mehra, V. Agarwal and S. K. Maji (2018). "Cytotoxic Oligomers and Fibrils Trapped in a Gel-like State of α-Synuclein Assemblies." Angewandte Chemie International Edition **57**(19): 5262-5266.

Laine, R. F., T. Sinnige, K. Y. Ma, A. J. Haack, C. Poudel, P. Gaida, N. Curry, M. Perni, E. A. Nollen and C. M. Dobson (2019). "Fast fluorescence lifetime imaging reveals the aggregation processes of α-synuclein and polyglutamine in aging Caenorhabditis elegans." ACS chemical biology **14**(7): 1628-1636.

Lautenschläger, J., A. D. Stephens, G. Fusco, F. Ströhl, N. Curry, M. Zacharopoulou, C. H. Michel, R. Laine, N. Nespovitaya and M. Fantham (2018). "C-terminal calcium binding of α-synuclein modulates synaptic vesicle interaction." Nature communications **9**(1): 1-13.

Li, B., P. Ge, K. A. Murray, P. Sheth, M. Zhang, G. Nair, M. R. Sawaya, W. S. Shin, D. R. Boyer and S. Ye (2018). "Cryo-EM of full-length α-synuclein reveals fibril polymorphs with a common structural kernel." Nature communications **9**(1): 1-10.

Longhena, F., G. Faustini, T. Varanita, M. Zaltieri, V. Porrini, I. Tessari, P. L. Poliani, C. Missale, B. Borroni and A. Padovani (2018). "Synapsin III is a key component of α-synuclein fibrils in Lewy bodies of PD brains." Brain Pathology **28**(6): 875-888.

591 Mahul-Mellier, A.-L., J. Burtscher, N. Maharjan, L. Weerens, M. Croisier, F. Kuttler, M.
592 Leleu, G. W. Knott and H. A. Lashuel (2020). "The process of Lewy body formation, rather
593 than simply α-synuclein fibrillization, is one of the major drivers of neurodegeneration."
594 Proceedings of the National Academy of Sciences **117**(9): 4971-4982.

595 Milovanovic, D., Y. Wu, X. Bian and P. De Camilli (2018). "A liquid phase of synapsin and
596 lipid vesicles." Science **361**(6402): 604-607.

597 Miskei, M., A. Horváth, M. Vendruscolo and M. Fuxreiter (2020). "Sequence-based
598 determinants and prediction of fuzzy interactions in protein complexes." Journal of Molecular
599 Biology.

600 Molliex, A., J. Temirov, J. Lee, M. Coughlin, A. P. Kanagaraj, H. J. Kim, T. Mittag and J. P.
601 Taylor (2015). "Phase separation by low complexity domains promotes stress granule assembly
602 and drives pathological fibrillization." Cell **163**(1): 123-133.

603 Murakami, T., S. Qamar, J. Q. Lin, G. S. K. Schierle, E. Rees, A. Miyashita, A. R. Costa, R.
604 B. Dodd, F. T. Chan and C. H. Michel (2015). "ALS/FTD mutation-induced phase transition
605 of FUS liquid droplets and reversible hydrogels into irreversible hydrogels impairs RNP
606 granule function." Neuron **88**(4): 678-690.

607 Nguyen, M. and D. Krainc (2018). "LRRK2 phosphorylation of auxilin mediates synaptic
608 defects in dopaminergic neurons from patients with Parkinson's disease." Proceedings of the
609 National Academy of Sciences **115**(21): 5576-5581.

610 Patel, A., H. O. Lee, L. Jawerth, S. Maharana, M. Jahnel, M. Y. Hein, S. Stoynov, J. Mahamid,
611 S. Saha and T. M. Franzmann (2015). "A liquid-to-solid phase transition of the ALS protein
612 FUS accelerated by disease mutation." Cell **162**(5): 1066-1077.

613 Poewe, W., K. Seppi, C. M. Tanner, G. M. Halliday, P. Brundin, J. Volkmann, A.-E. Schrag
614 and A. E. Lang (2017). "Parkinson disease." Nature reviews Disease primers **3**(1): 1-21.

615 Pogostin, B. H., S. Linse and U. Olsson (2019). "Fibril Charge Affects α-Synuclein Hydrogel
616 Rheological Properties." Langmuir **35**(50): 16536-16544.

617 Polymeropoulos, M. H., C. Lavedan, E. Leroy, S. E. Ide, A. Dehejia, A. Dutra, B. Pike, H.
618 Root, J. Rubenstein and R. Boyer (1997). "Mutation in the α-synuclein gene identified in
619 families with Parkinson's disease." science **276**(5321): 2045-2047.

620 Poudel, C., I. Mela and C. F. Kaminski (2020). "High-throughput, multi-parametric, and
621 correlative fluorescence lifetime imaging." Methods and Applications in Fluorescence **8**(2):
622 024005.

623 R. Bodner, C., C. M. Dobson and Ad Bax (2009). "Multiple Tight Phospholipid-Binding
624 Modes of α-Synuclein Revealed by Solution NMR Spectroscopy." <u>Journal of Molecular</u>
625 <u>Biology</u> **390**(4): 775-790.

626 Ray, S., N. Singh, R. Kumar, K. Patel, S. Pandey, D. Datta, J. Mahato, R. Panigrahi, A.
627 Navalkar, S. Mehra, L. Gadhe, D. Chatterjee, A. S. Sawner, S. Maiti, S. Bhatia, J. A. Gerez,
628 A. Chowdhury, A. Kumar, R. Padinhateeri, R. Riek, G. Krishnamoorthy and S. K. Maji (2020).
629 "α-Synuclein aggregation nucleates through liquid–liquid phase separation." <u>Nature</u>
630 <u>Chemistry</u>.

631 Schapira, A. H., C. W. Olanow, J. T. Greenamyre and E. Bezard (2014). "Slowing of
632 neurodegeneration in Parkinson's disease and Huntington's disease: future therapeutic
633 perspectives." <u>The Lancet</u> **384**(9942): 545-555.

634 Schweighauser, M., Y. Shi, A. Tarutani, F. Kametani, A. G. Murzin, B. Ghetti, T. Matsubara,
635 T. Tomita, T. Ando and K. Hasegawa (2020). "Structures of α-synuclein filaments from
636 multiple system atrophy." <u>BioRxiv</u>.

637 Shahmoradian, S. H., A. J. Lewis, C. Genoud, J. Hench, T. E. Moors, P. P. Navarro, D.
638 Castaño-Díez, G. Schweighauser, A. Graff-Meyer and K. N. Goldie (2019). "Lewy pathology
639 in Parkinson's disease consists of crowded organelles and lipid membranes." <u>Nature</u>
640 <u>neuroscience</u> **22**(7): 1099-1109.

641 Shin, Y. and C. P. Brangwynne (2017). "Liquid phase condensation in cell physiology and
642 disease." <u>Science</u> **357**(6357): eaaf4382.

643 Singleton, A., M. Farrer, J. Johnson, A. Singleton, S. Hague, J. Kachergus, M. Hulihan, T.
644 Peuralinna, A. Dutra and R. Nussbaum (2003). "α-Synuclein locus triplication causes
645 Parkinson's disease." <u>Science</u> **302**(5646): 841-841.

646 Sinnige, T., G. Meisl, T. C. T. Michaels, M. Vendruscolo, T. P. J. Knowles and R. I. Morimoto
647 (2020). "Kinetic analysis reveals the rates and mechanisms of protein aggregation in a
648 multicellular organism." <u>bioRxiv</u>: 2020.2008.2013.249862.

649 Spillantini, M. G., R. A. Crowther, R. Jakes, M. Hasegawa and M. Goedert (1998). "-Synuclein
650 in filamentous inclusions of Lewy bodies from Parkinson's disease and dementia with Lewy
651 bodies." <u>Proceedings of the National Academy of Sciences</u> **95**(11): 6469-6473.

652 Spillantini, M. G., R. A. Crowther, R. Jakes, M. Hasegawa and M. Goedert (1998). "α-
653 Synuclein in filamentous inclusions of Lewy bodies from Parkinson's disease and dementia
654 with Lewy bodies." <u>Proceedings of the National Academy of Sciences</u> **95**(11): 6469-6473.

655 Spillantini, M. G., M. L. Schmidt, V. M.-Y. Lee, J. Q. Trojanowski, R. Jakes and M. Goedert
656 (1997). "α-Synuclein in Lewy bodies." <u>Nature</u> **388**(6645): 839-840.

657 Takamori, S., M. Holt, K. Stenius, E. A. Lemke, M. Grønborg, D. Riedel, H. Urlaub, S.
658 Schenck, B. Brügger and P. Ringler (2006). "Molecular anatomy of a trafficking organelle."
659 Cell **127**(4): 831-846.

660 Taschenberger, G., M. Garrido, Y. Tereshchenko, M. Bähr, M. Zweckstetter and S. Kügler
661 (2012). "Aggregation of αSynuclein promotes progressive in vivo neurotoxicity in adult rat
662 dopaminergic neurons." Acta Neuropathol **123**(5): 671-683.

663 Valera, E. and E. Masliah (2016). "Therapeutic approaches in Parkinson's disease and related
664 disorders." Journal of neurochemistry **139**: 346-352.

665 Van Ham, T. J., K. L. Thijssen, R. Breitling, R. M. Hofstra, R. H. Plasterk and E. A. Nollen
666 (2008). "C. elegans model identifies genetic modifiers of α-synuclein inclusion formation
667 during aging." PLoS genetics **4**(3).

668 Van Ham, T. J., K. L. Thijssen, R. Breitling, R. M. W. Hofstra, R. H. A. Plasterk and E. A. A.
669 Nollen (2008). "C. elegans Model Identifies Genetic Modifiers of α-Synuclein Inclusion
670 Formation During Aging." PLoS Genetics **4**(3): e1000027.

671 Visanji, N. P., J. M. Brotchie, L. V. Kalia, J. B. Koprich, A. Tandon, J. C. Watts and A. E.
672 Lang (2016). "α-Synuclein-Based Animal Models of Parkinson's Disease: Challenges and
673 Opportunities in a New Era." Trends Neurosci **39**(11): 750-762.

674 Volpicelli-Daley, L. A., K. C. Luk and V. M. Lee (2014). "Addition of exogenous α-synuclein
675 preformed fibrils to primary neuronal cultures to seed recruitment of endogenous α-synuclein
676 to Lewy body and Lewy neurite-like aggregates." Nat Protoc **9**(9): 2135-2146.

677 Wakabayashi, K., K. Tanji, S. Odagiri, Y. Miki, F. Mori and H. Takahashi (2013). "The Lewy
678 Body in Parkinson's Disease and Related Neurodegenerative Disorders." Molecular
679 Neurobiology **47**(2): 495-508.

680 Warren, S. C., A. Margineanu, D. Alibhai, D. J. Kelly, C. Talbot, Y. Alexandrov, I. Munro, M.
681 Katan, C. Dunsby and P. M. French (2013). "Rapid global fitting of large fluorescence lifetime
682 imaging microscopy datasets." PLoS One **8**(8).

683 Wegmann, S., B. Eftekharzadeh, K. Tepper, K. M. Zoltowska, R. E. Bennett, S. Dujardin, P.
684 R. Laskowski, D. MacKenzie, T. Kamath and C. Commins (2018). "Tau protein liquid–liquid
685 phase separation can initiate tau aggregation." The EMBO journal **37**(7).

686 Yuan, C., A. Levin, W. Chen, R. Xing, Q. Zou, T. W. Herling, P. K. Challa, T. P. Knowles and
687 X. Yan (2019). "Nucleation and Growth of Amino Acid and Peptide Supramolecular Polymers
688 through Liquid–Liquid Phase Separation." Angewandte Chemie **131**(50): 18284-18291.

689 Zaltieri, M., J. Grigoletto, F. Longhena, L. Navarria, G. Favero, S. Castrezzati, M. A.
690 Colivicchi, L. Della Corte, R. Rezzani and M. Pizzi (2015). "α-synuclein and synapsin III
691 cooperatively regulate synaptic function in dopamine neurons." J Cell Sci **128**(13): 2231-2243.
692
693
694
695
696

697
698
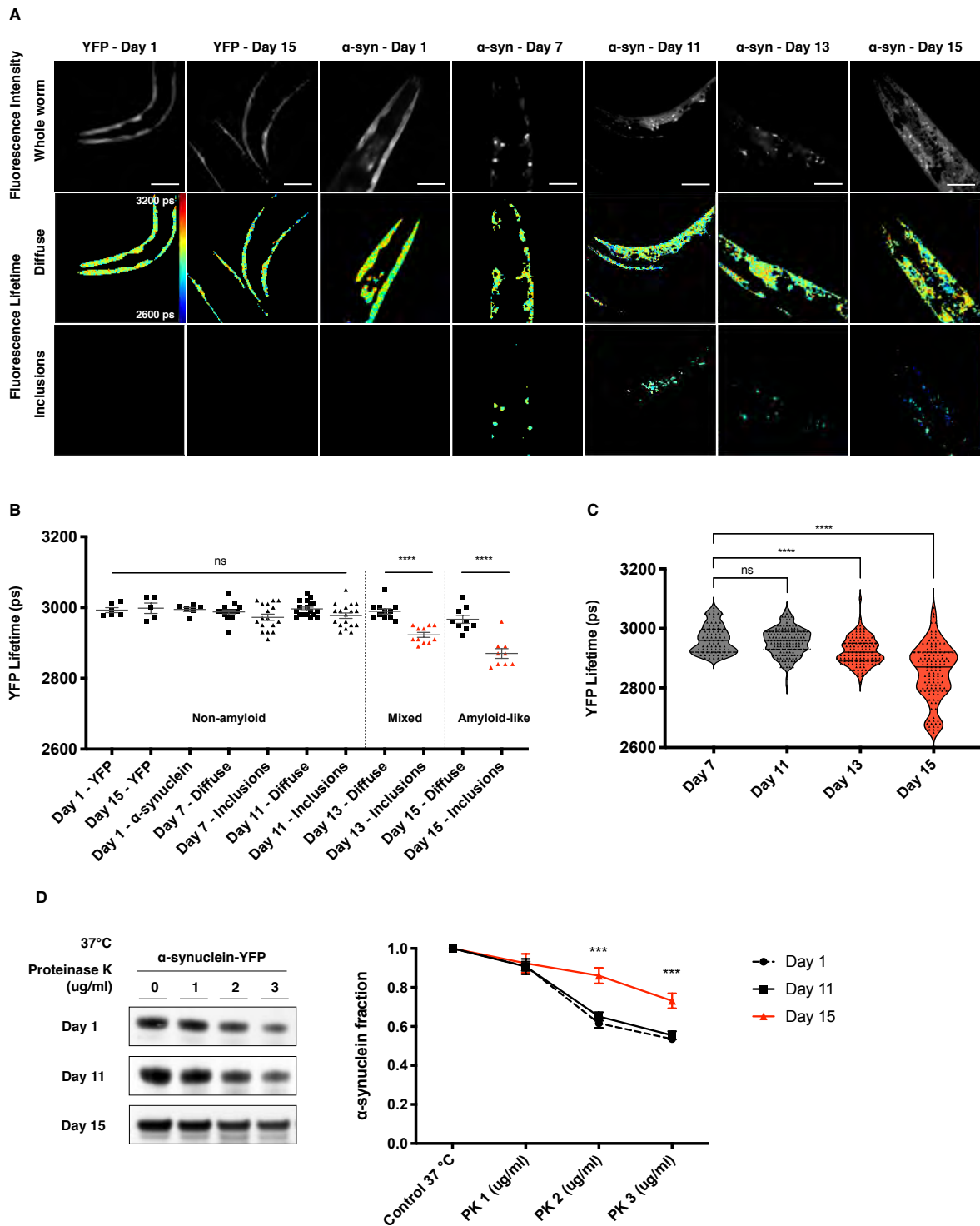
Figure 1. α-Synuclein forms non-amyloid inclusions in *C. elegans*. (A) Age-dependent coalescence of α-synuclein-YFP in body wall muscle cells into cytoplasmic inclusions, with distinct lifetime profiles between inclusions and diffuse signal. The scale bar represents 25 μm, rainbow scale bar 2600 (blue) - 3200 (red) picoseconds (ps). **(B)** Analysis of the high-resolution FLIM revealing that α-synuclein assemblies are predominantly non-amyloid in *C. elegans*. At

704 day 13 and 15 a shift towards lifetimes associated with the amyloid-state can be observed. No
705 shift can be observed for worms expressing only YFP. Each square and triangle represents one
706 animal from the population. **(C)** Violin plots for all individual inclusions from the animals in
707 (B). A distinct population of lower lifetime inclusions appears at old age. Black line = median.
708 Dotted line = quartiles. **(D)** Appearance of proteinase K resistant protein species show α-
709 synuclein-YFP with increased amyloid-like self-association in aged animals (days 13-15 of
710 adulthood). α-Synuclein levels probed with the LB509 antibody (Methods) are shown (*left*).
711 Quantification of protein levels corrected for loading control and normalised against untreated
712 control (*right*). Results are mean ± SEM. One-way ANOVA. ***$P \leq 0.001$, ****$P \leq 0.0001$,
713 ns, not significant.

714
715
716
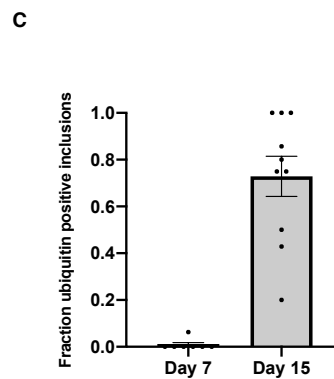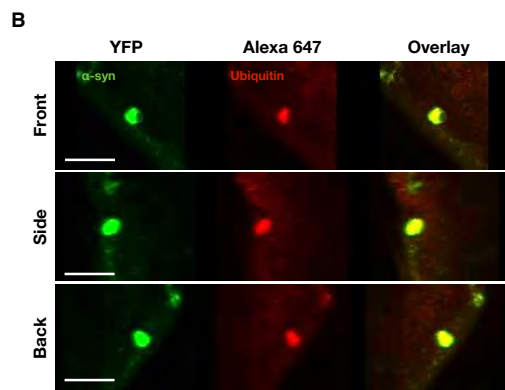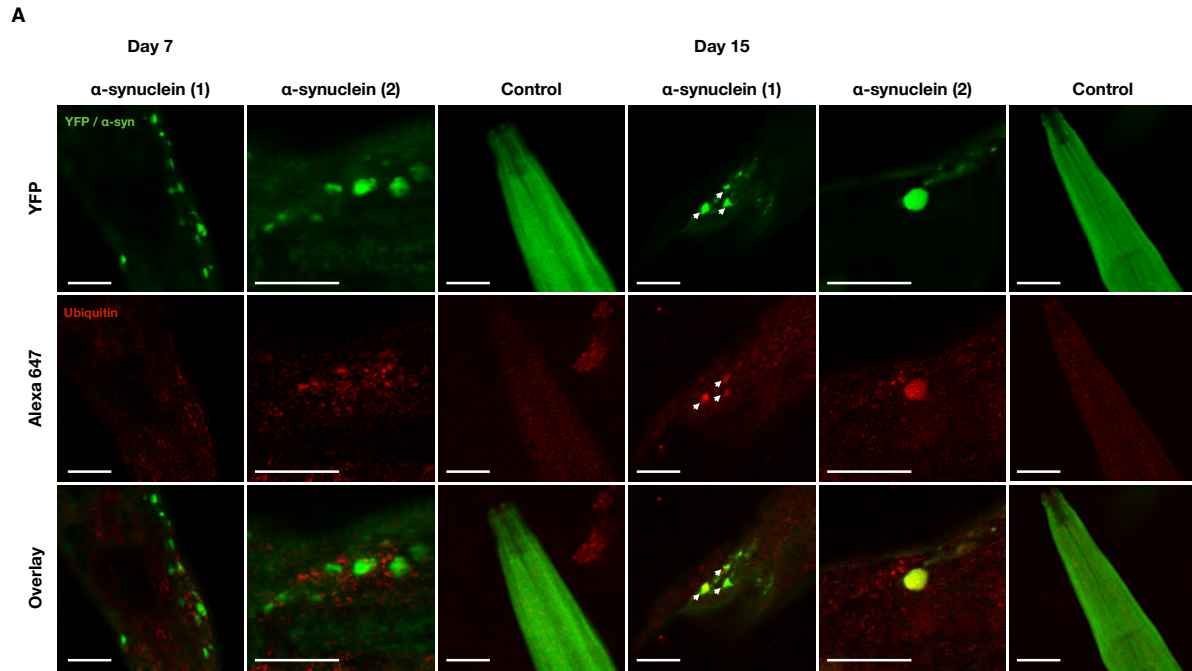
717
718
Figure 2. α-Synuclein inclusions in aged worms are immunoreactive for ubiquitin. (**A**) Inclusions in aged worms (day 15, *right*) are immunoreactive for ubiquitin, whereas inclusions in younger worms (day 7, *left*) show no immunoreactivity. For each time point, two representative animals are shown together with a control strain expressing only YFP. The scale bars represent 20 μm. (**B**) 3D rendering of an image stack, showing co-localisation of α-synuclein-YFP and Alexa 647 anti-ubiquitin signal in an aged worm (day 15). The scale bar represents 10 μm. (**C**) Quantification of ubiquitin positive inclusions at indicated timepoints. Each datapoint represents the average number of ubiquitin positive inclusions in one worm. Results are mean + SEM.
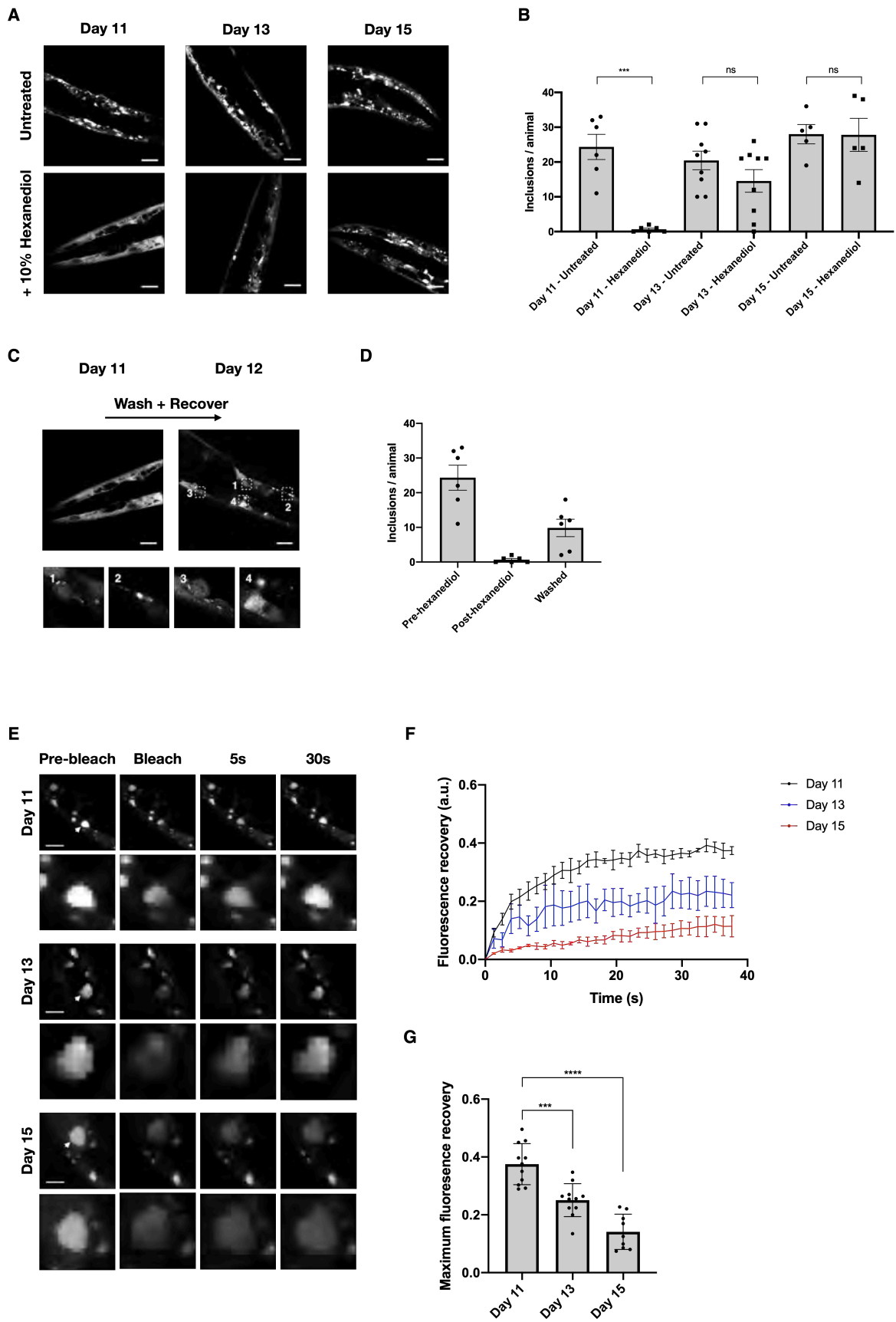
728

729 **Figure 3. Early α-synuclein inclusions in *C. elegans* have liquid-like properties**. **(A)**

730 Exposure to 10% (w/v) 1,6-hexanediol dissolves α-synuclein inclusions in body wall muscle

731 cells between days 1 and 11 of adulthood, reflecting the dependence of inclusion assembly on
732 weak hydrophobic interactions. By contrast, inclusions in aged nematodes (days 13-15 of
733 adulthood) appear to be amyloid-like, as evidenced by decreased hexanediol efficacy. **(B)**
734 Quantification of images in (A). Each square or circle represents one animal from the
735 population. **(C)** α-Synuclein assemblies in younger nematodes reappear after hexanediol is
736 washed out. Newly formed small inclusions were observed in washed worms after one day of
737 recovery, reflecting the dynamic and liquid-like nature of α-synuclein assemblies in *C. elegans.*
738 **(D)** Quantification of images in **(C)**. The scale bars represent 25 μm. **(E)** Fluorescent recovery
739 after photobleaching (FRAP) of α-synuclein inclusions at indicated timepoints. Scale bars
740 represent 10 μm. **(F)** Average recovery trace of all inclusions in a single worm, at indicated
741 timepoints. Error bars represent SEM. **(G)** Maximum fluorescent recovery at indicated
742 timepoints. Each datapoint represents the average maximum recovery of all inclusions in a
743 single worm. Results are mean ± SEM. One-way ANOVA. ***$P \leq 0.001$, ****$P \leq 0.0001$, ns,
744 not significant.
745
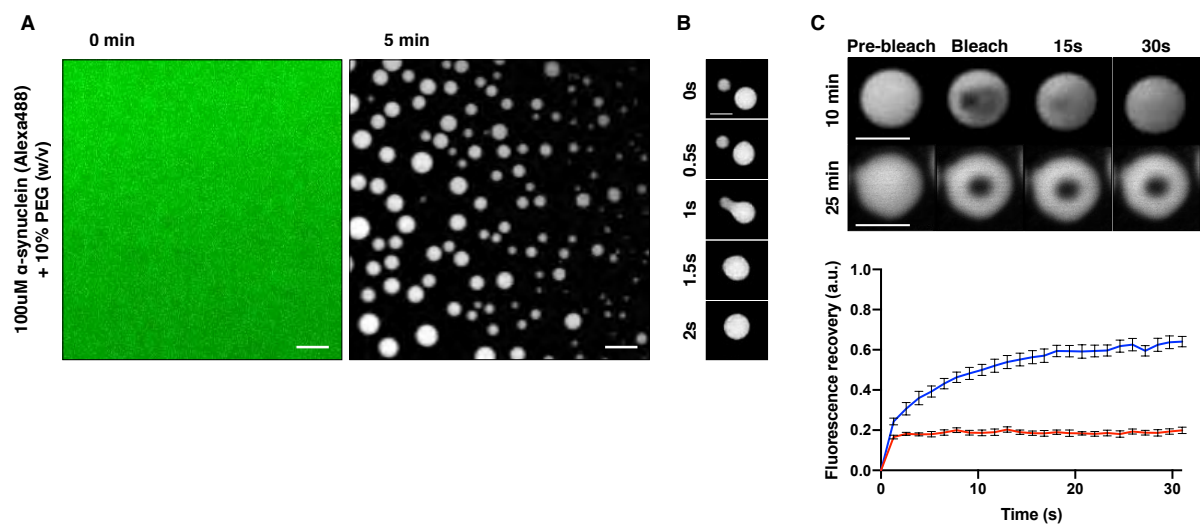
Figure 4. α-Synuclein undergoes liquid-liquid phase separation *in vitro*. (A) Wild-type human α-synuclein (100 μM) in the presence of 10% PEG, supplemented with 1 mol% Alexa-488 labelled α-synuclein, forms micrometre sized droplets under physiological conditions. The scale bar represents 5 μm. **(B)** Fusion of two α-synuclein droplets in close proximity (<1 μm). The scale bar represents 1 μm. **(C)** Fluorescence recovery after photobleaching (FRAP) of a small area within the droplet. Red line represents aged droplets. The scale bar represents 1 μm; error bars represent SEM.

768
769
770 **Figure 5. α-Synuclein droplets mature into amyloid-like hydrogels under *in vitro*. (A)** α-
771 Synuclein in the presence of 10% PEG becomes turbid, representing the formation of light-
772 scattering objects such as droplets. Data points represent 5 min interval measurements,
773 preceded by brief shaking. **(B)** α-Synuclein becomes positive for ThT following an increase in
774 turbidity, indicating that the assemblies adopt an amyloid-like nature. **(C)** Scanning electron
775 microscopy (cryo-SEM) image of α-synuclein hydrogel, formed at the end of the experiment
776 shown in (B). Left panel shows the hydrogel. The morphology as seen by cryo-SEM (middle
777 and right panels) indicates that hydrogels are rich in fibrillar structures. The scale bars represent
778 1 μm *(left)* and 500 nm *(right)*.

779
780
781
782
783
784
785
786
787

788
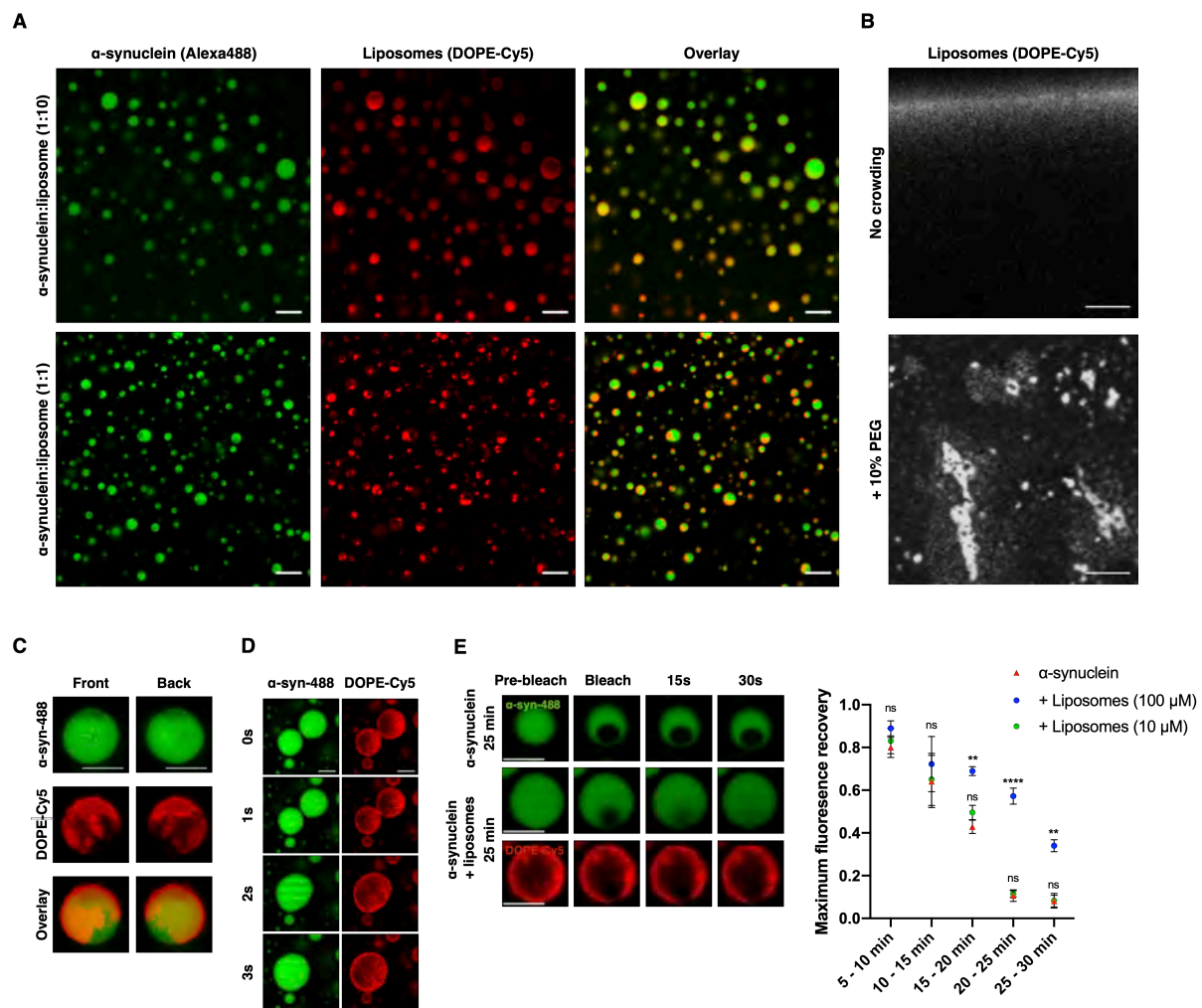
Figure 6. α-Synuclein droplets co-localise with liposomes. **(A)** α-Synuclein droplets co-localise with liposomes resembling the lipid composition of synaptic vesicles (DOPE:DOPC:DOPS) labelled with DOPE-Cy5. α-Synuclein (100 μM) was incubated with either 1mM (protein:lipid, 1:10, *top)* or 100 μM liposomes (protein:lipid, 1:1, *bottom).* The scale bars represent 5 μm. **(B)** Liposomes (1mM) in buffer remain diffuse (*top*) or form aggregates (*bottom*). The scale bar represents 10 μm. **(C)** 3D rendering of the droplets showing that lipids are directly recruited into α-synuclein droplets (protein:lipid, 1:1). The scale bar represents 1 μm. **(D)** Fusion of two α-synuclein/liposome droplets in close proximity (protein:lipid, 1:1).. The scale bar represents 1 μm. **(E)** α-synuclein/liposome droplets mature slower than droplets containing only α-synuclein (protein:lipid, 1:1). Lowering the protein:lipid ratio to 10:1 results in a loss of the protective effect. Each data point represents the average recovery out of three droplets for that timeframe. The scale bar represents 1 μm; error bars represent SEM. One-way ANOVA. **$*P \leq 0.01$, ****$P \leq 0.0001$, ns, not significant.
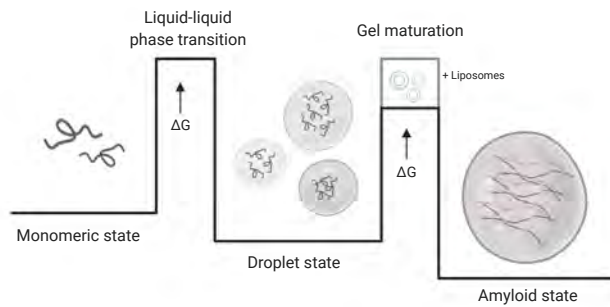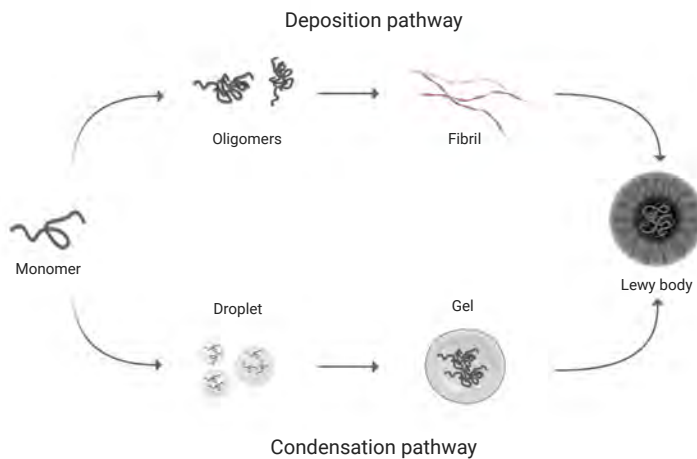
802

803

804 **Figure 7. Schematic illustration of the possible deposition and condensation pathways of**
805 **α-synuclein self-assembly into Lewy bodies. (A)** α-Synuclein can populate the monomeric
806 state, the droplet state and the amyloid state. The amyloid state is likely to be the
807 thermodynamically most stable state under cellular conditions, but its kinetic accessibility is
808 reduced by the presence of free energy barriers between the native and droplet states, and by
809 the droplet and amyloid states. The latter free energy barrier can be crossed through a
810 maturation process that involves the formation of gel-like amyloid-rich assemblies that
811 gradually age into the amyloid state. This slow conversion can become altogether arrested in
812 the presence of cellular components, possibly resulting in the formation of Lewy bodies. **(B)**
813 The conversion of α-synuclein from the monomeric to the amyloid state can proceed through
814 two distinct pathways. In the 'deposition pathway', α-synuclein forms initially small disordered
815 oligomers that then convert into ordered oligomers, which then grow into amyloid fibrils. In
816 the 'condensation pathway' α-synuclein forms first a droplet state, which then gradually mature

817 into the amyloid state going through gel intermediates. Although both pathways can be
818 homogeneous, with α-synuclein as the sole component of the system, in complex environments
819 they are most likely heterogeneous, with other cellular components taking part in the process,
820 including in particular lipid membranes
821
822
823
824
825
826
827
828
829
830
831
832
833
834
835
836
837
838
839
840
841
842
843
844
845
846
847
848
849
850
851
852
853
854

855

856
857

858
859
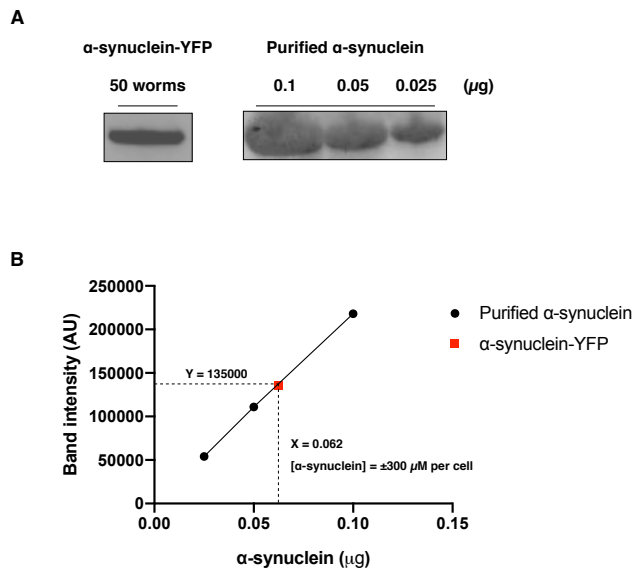
Figure S1. Determination of α-synuclein concentration in *C. elegans* body wall muscle cells. **(A)** Protein concentration in body wall muscle cells was determined by immunoblotting a known number of worms and comparing the protein band intensity against standard with purified α-synuclein. **(B)** Comparison of the protein band intensity results in 0.062 μg protein in the tested sample. When converted to the concentration per single body wall muscle cell (see **Methods)**, this concentration is ±300 μM.

866
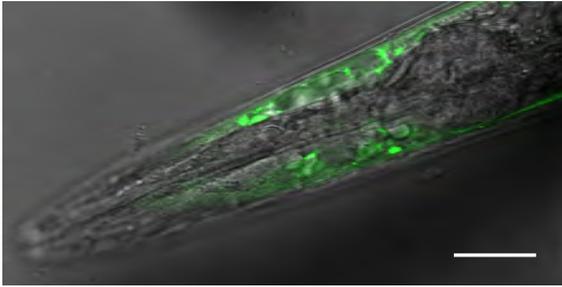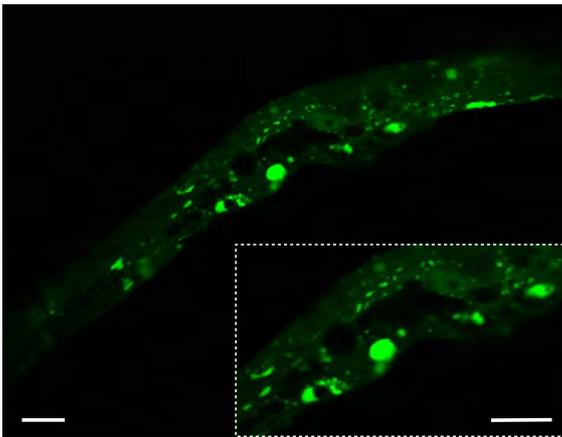
868

869

870 **Figure S2. Localisation of human α-synuclein-YFP in *C. elegans* body wall muscle cells**.

871 **(A)** Confocal image detailing the localisation of α-synuclein-YFP (*green*), expressed in body

872 wall muscle cells. Scale bar represents 30 μm. **(B)** Magnified confocal image showing the

873 subcellular localisation of both diffuse α-synuclein-YFP and α-synuclein-YFP inclusions at

874 body wall muscle cells. Scale bars represent 5 μm.

875

876

877
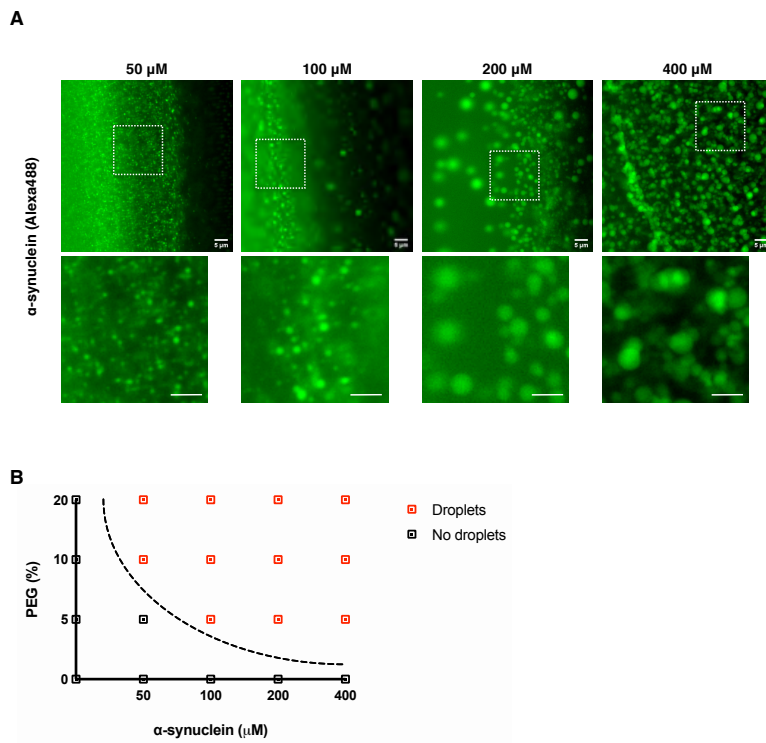
Figure S3. α-Synuclein forms droplets at various concentrations under crowding conditions. (A) Wide field microscopy images of α-synuclein forming micrometre-sized droplets in the presence of 10% PEG after 5 minutes incubation. Droplet size scales with protein concentration. The scale bar represents 5 μm. **(B)** Phase diagram of the droplet state as a function of α-synuclein and PEG concentration at 5 minutes post incubation. Dotted line represents theoretical phase-barrier, based on experimental observations.


884

885

886

887

888

889

890

891

892
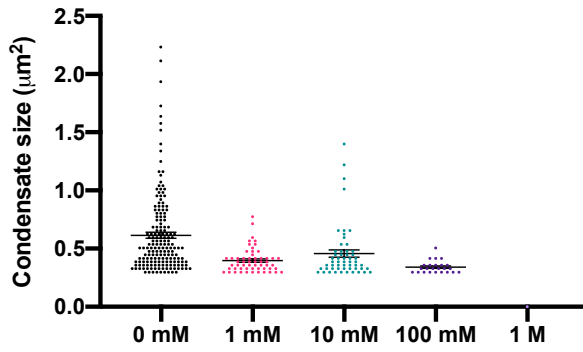
Figure S4. α-Synuclein droplet formation is sensitive to solution ionic strength. Dose-dependent distribution graphs representing the quantification of the effects of NaCl on the average size of condensates, 5 minutes post incubation of 50 µM α-synuclein in the presence of 10% PEG and indicated NaCl concentration. Each data point represents the size of one individual condensate.

898

899

900

901

902

903

904

905

906

907

908

909

910

911

A Binding mode

B Droplet formation
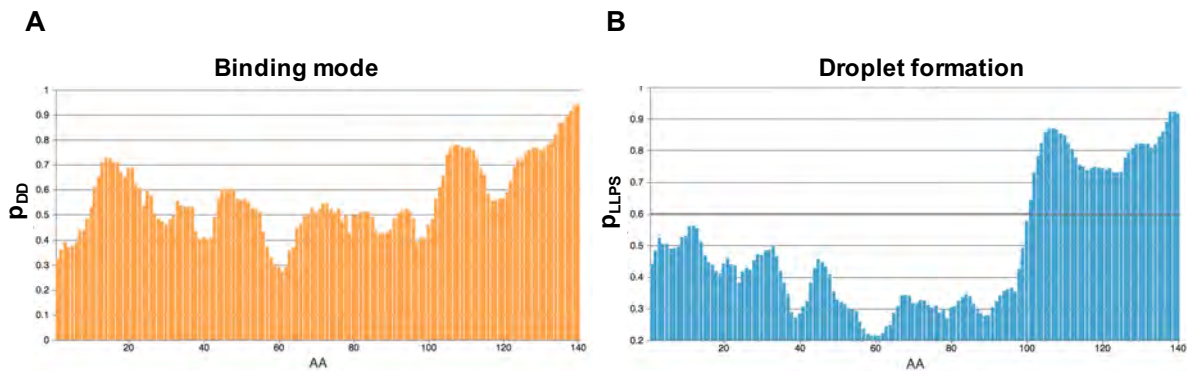
912

913

914 **Figure S5. The acidic C-terminal region of α-synuclein likely drives droplet formation**

915 **through disordered interactions.** (**A**) A sequence-based prediction of the binding modes of

916 disordered α-synuclein (Miskei, Horváth et al. 2020) suggests that the C-terminus remains

917 predominantly disordered (p_{DD}, orange) in complexes with other disordered proteins, including

918 α-synuclein. (**B**) A sequence-based prediction of the probability of spontaneous liquid-liquid

919 phase separation (p_{LLPS}) indicates an important role for the C-terminus of α-synuclein in droplet

920 formation (protdyn-fuzpred.org).

921

922

923

924

925

926

927

928

929

930

931

932

933

934

935

936

937

938

939 **Movie S1.** 1,6-hexanediol dissolves non-amyloid α-synuclein inclusions in *C. elegans*. 3D
940 rendering of living animals showing α-synuclein-YFP at body wall muscle cells. Control (*left*)
941 represents untreated animal. Hexanediol (*right*) represents animal treated with 10% (w/v) 1,6
942 hexanediol.

943

944 **Movie S2.** Rapid droplet formation of α-synuclein (100 μM) in the presence of 10% PEG after
945 deposition on a glass slide starting at the edge of the solution (lag time ±60s) and spreading
946 inwards. Droplets sediment on the glass surface over time. The scale bar represents 5 μm.

947

948 **Movie S3.** Fusion event of two α-synuclein droplets after 5 min incubation. The scale bar
949 represents 1 μm.

950

951 **Movie S4.** Fluorescence recovery of α-synuclein after photobleaching of a region within a
952 droplet.

953

954 **Movie S5**. Droplet formation of α-synuclein (100 μM) incubated with 1mM (protein:lipid,
955 1:10) DOPE:DOPC:DOPS liposomes (1 mol% DOPE-Cy5) in the presence of 10% PEG,
956 starting at the edge of the solution and spreading inwards (lag time ±40s). Liposomes initially
957 localise on the edge of α-synuclein droplets (t=100s), before completely mixing (t=200s).
958 Channels represent α-synuclein (*left*), liposomes (*middle*) and an overlay (*right*). Scale bar
959 represents 5 μm.

960

961 **Movie S6.** 3D rendering of a z-stack of a single α-synuclein/lipid droplet. Channels represent
962 an overlay (*left*), α-synuclein (*middle*) and lipids (*right*). Scale bar represents 1 μm.

963

964